ACS APPLIED ENGINEERING MATERIALS

pubs.acs.org/acsaenm Letter

# Carbon Dioxide Adsorption within Porous Porphyrin Networks

Syed Ibrahim Gnani Peer Mohamed,[§] Sarang Ismail,[§] Ahmed El-Harairy, Mona Bavarian,* and Siamak Nejati*

Cite This: *ACS Appl. Eng. Mater.* 2024, 2, 1743−1747 Read Online

ACCESS | Metrics & More | Article Recommendations | Supporting Information

**ABSTRACT:** Porphyrin-based films containing nanoscale crystallites of covalent organic frameworks (MPOR-COFs, where M = $H_2$, $Cu^{2+}$, $Zn^{2+}$) have been synthesized, and their adsorption properties have been studied. The adsorption isotherms for $CO_2$ indicate distinct variations in adsorption energetics and capacity among films prepared with different porphyrin precursors. $H_2$POR-COF films exhibited enhanced $CO_2$ capture performance compared to those containing zinc and copper in their porphyrin rings. The heat of adsorption and the adsorption capacity for the metal-free films were about 50% lower and 100% higher than those of the metal-containing films. Increased crystallinity in the films was found to reduce their $CO_2$ adsorption capacities. This work highlights the viability of our synthetic approach to create tunable porphyrin-based frameworks for gas separation applications.

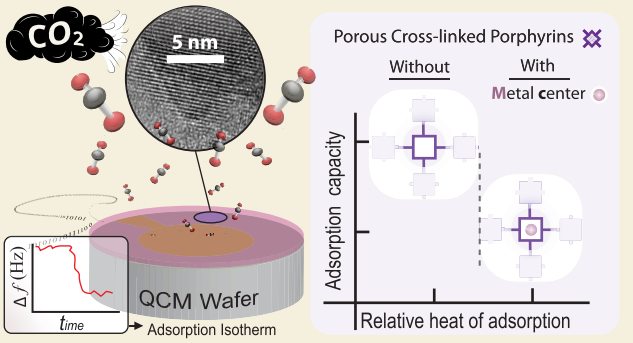


**KEYWORDS:** *Carbon dioxide, porous organic polymer, gas sorption, green chemistry, global warming, vapor phase polymerization*



Escalating atmospheric carbon dioxide ($CO_2$) levels and their detrimental impacts on global climate have intensified the quest for efficient $CO_2$ capture technologies.[1] Various porous materials, including Zeolite,[2] activated carbon,[3] and metal−organic frameworks (MOFs),[4] have emerged as promising candidates for $CO_2$ capture. However, Zeolite faces challenges such as reduced $CO_2$ capture efficiency in moist conditions due to water saturation, limited pore volume, and the need for regeneration at high temperatures.[5,6] Similarly, activated carbon encounters issues related to pore engineering and low $CO_2$ selectivity, and MOFs are constrained in $CO_2$ capture under humid conditions; the metal sites within MOFs exhibit a stronger affinity for water bonding over $CO_2$.[7] Therefore, searching for cost-effective and stable $CO_2$ capture material has been ongoing.

Along these lines, covalent organic frameworks (COFs) have emerged as promising materials for $CO_2$ capture due to their high surface area, tunable pore structures, and chemical stability.[8] Among COFs, porphyrin-based COFs have garnered significant attention because of the high affinity of porphyrin units for $CO_2$ molecules.[9] Porphyrins are extensively explored in various applications, including catalysis,[10] sensing,[11] and photovoltaics.[12] It is predicted that incorporating porphyrin into COFs offers a path to introduce functionalities that can be tuned to enhance $CO_2$ sorption performance.[13]

Herein, we evaluate the $CO_2$ sorption capacity of thin polymeric films containing porphyrin-based covalent organic frameworks (MPOR-COFs, where M= $H_2$, $Cu^{2+}$, $Zn^{2+}$), synthesized via a bottom-up vapor-phase oxidative polymerization technique. Here, M = $H_2$ is referred to as POR-COF, M = $Cu^{2+}$ as CuPOR-COF, and M = $Zn^{2+}$ as ZnPOR-COF, respectively. Our findings reveal that the POR-COF exhibits enhanced $CO_2$ capture performance compared with ZnPOR-COF and CuPOR-COF. These findings highlight the tunability of porphyrin-based COFs, providing valuable insights for developing separation media for carbon dioxide separation.

To deposit thin films of MPOR-COFs, porphyrin molecules, namely 5,10,15,20-tetra(4-aminophenyl) porphyrin (TAPP) or its transition-metal complexes (M-TAPP, where M = $Zn^{2+}$, $Cu^{2+}$), were prepared, purified, and employed as the primary precursors. The preparation procedure for TAPP and Cu-TAPP is outlined in our prior publication,[14] and the procedure for Zn-TAPP is provided in Supporting Information, Section 1. The corresponding structural characterization and thermal stability of Zn-TAPP are provided in Figures S1−S3. A quartz crystal microbalance (QCM) crystal (PhillipTech, 6 MHz, 14 mm, gold AT cut) was pretreated by washing with isopropyl alcohol (IPA), dried using nitrogen, and then loaded into the reactor, which was subsequently evacuated to its base pressure. The oxidant, antimony pentachloride ($SbCl_5$, 99%, Thermo

Received: April 26, 2024
Revised: July 1, 2024
Accepted: July 2, 2024
Published: July 5, 2024

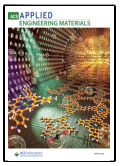




https://doi.org/10.1021/acsaenm.4c00285
*ACS Appl. Eng. Mater.* 2024, 2, 1743−1747

Scientific), and pyridine (dry, Sigma-Aldrich) were placed in a Pyrex-metal jar and introduced into the reactor using a precise needle valve (Swagelok). The reactor pressure was monitored using the MKS 946 vacuum system controller. The monomer was sublimated from a low-temperature evaporator (LTE), followed by a 5 min waiting period to allow the adsorption of the monomer onto the substrate. The reactor was then evacuated to its base pressure using argon purging. Subsequently, an oxidant pulse was given for ten seconds (increasing the pressure to 15 to 20 mTorr), followed by evacuating the chamber to its base pressure using argon purging. This deposition process was repeated for 10 cycles. In instances where pyridine was introduced, a pyridine pulse preceded the introduction of the monomer, followed by the oxidant pulse. The resulting MPOR-COF synthesized with a pyridine pulse was denoted as POR-COF-Py, ZnPOR-COF-Py, and CuPOR-COF-Py, respectively. The plausible reaction mechanism for MPOR-COFs formation is discussed in our previous publication.[14] Briefly, the amine group at the meso position forms an adduct with $SbCl_5$, directing to subsequent two-electron oxidation. This oxidation leads to forming a radical cation (M-TAPP $^{\cdot+}$) from M-TAPP. The intermediate is stabilized by $Cl^-$ ions through the elimination of two protons. These radical cations then undergo coupling reactions, forming dihydrophenazine or phenazine linkages. When two neighboring radical cations react, dimers or higher oligomers are formed. This polymerization process continues as dimers or oligomers react further, propagating the polymer chain. The process continues until termination occurs, yielding the final polymer product. Additionally, pyridine acted as a mild base to neutralize the HCl byproduct. For measuring $CO_2$ adsorption, the samples were coated on QCM substrate using different coating conditions. Figure 1 illustrates the schematic

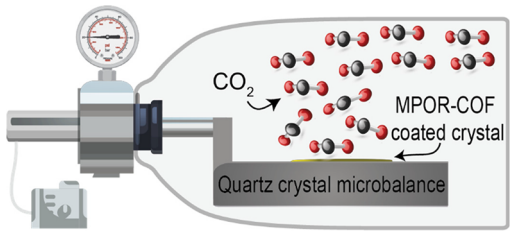


**Figure 1.** Schematic representation of the $CO_2$ adsorption measurement using quartz crystal microbalance (QCM).

representation of the $CO_2$ adsorption method we employed. Our experimental setup was designed based on the original work of Baltus et al., utilizing QCM measurements for sorption studies.[15] Here, a high-pressure cell equipped with a QCM module is used to assess the adsorption of $CO_2$ in our films.

Figure 2A and Figure S4 provide AFM height images, comparing the surface characteristics of pristine and ZnPOR-COF-coated QCM crystals. As shown, the pristine QCM crystal is observed to possess an average surface roughness (Ra) measuring 1.8 nm. In contrast, the ZnPOR-COF-coated QCM crystal demonstrates a marginal increase in Ra, measuring at 4.5 nm. Figure S5 in the supporting infromation displays the AFM height images of other samples coated on QCM crystals, and the digital photographic images of both pristine and POR-COF-coated QCM crystals are shown in Figure S6. The crystalline property of the synthesized MPOR-COF on sapphire was analyzed using powder X-ray diffraction (PXRD) and transmission electron microscopy (TEM). As illustrated in Figure 2B, the PXRD spectra of ZnPOR-COF and ZnPOR-COF-Py showcase a distinct peak at around 28°, ascribed to the (001) plane. The degree of crystallinity was determined by computing the ratio of the integrated area of all crystalline peaks to the total integrated area beneath the PXRD peaks. The crystallinity analysis reveals that ZnPOR-COF exhibits a degree of crystallinity of approximately 36%. This value was notably increased to 51% for ZnPOR-COF-Py, indicating a significant improvement attributed to including pyridine pulse during the oxidative polymerization. This trend is similar to our previous observation of POR-COF-Py and CuPOR-COF-Py crystallinity prepared using comparable conditions.[14] TEM examination, portrayed in Figure 2C, further substantiates these findings, unveiling well-defined lattice patterns with crystalline domains as large as 20 nm within the deposited films, characterized by consistent orientations. Correspondingly, the TEM analysis of POR-COF-Py and CuPOR-COF-Py (demonstrated in Figure S7) present aligned lattice structures, indicative of their inherent crystalline nature. Moreover, determining lattice fringe spacing for ZnPOR-COF-Py, POR-COF-Py, and CuPOR-COF-Py yields values of 0.3, 0.29, and 0.3 nm, respectively, closely aligning with the PXRD data.

The deposited materials on QCM crystals were further characterized for their chemical properties and environment. As shown in Figure 2D, the Zn-TAPP precursor showcased asymmetric and symmetric stretching of primary amine ($-NH_2$) at 3422 and 3324 $cm^{-1}$, respectively, along with the N−H bending vibration observed at 1614 $cm^{-1}$.[16] Porphyrin-specific stretching associated with −CH out-of-plane bending and in-plane bending were identified at 712, 730, 794, 972, 988, and 1059 $cm^{-1}$, respectively.[16] Additionally, characteristic peaks at 1340, 1419, and 1472 $cm^{-1}$ were attributed to pyrrole skeletal stretching. Following oxidative polymerization, the C-NH-C bending, an indication of cross-coupling of the precursor molecules, was observed at 1285 $cm^{-1}$.[17] The complete ATR-FTIR characterization of POR-COF and CuPOR-COF on the QCM crystal is detailed in Figure S8. The peak associated with the asymmetric stretching of primary amine groups remained visible, suggesting that the reactions were incomplete. The chemical bonding present within ZnPOR-COF was also analyzed using X-ray photoelectron spectroscopy (XPS). As shown in Figure 2E, the N 1s high-resolution XPS spectrum of ZnPOR-COF is deconvoluted into four distinct peaks centered at 398.6, 399.5, 401.1, and 402.0 eV, which can be assigned to nonprotonated pyrrolic N, dihydrophenazine N, N-oxide, and a satellite peak, respectively.[18−20] The UV−Vis absorption spectra of Zn-TAPP and ZnPOR-COF deposited on quartz are depicted in Figure 2F. While Zn-TAPP displays distinct peaks with the Soret band observed at 430 nm and Q bands at 546 and 587 nm, ZnPOR-COF exhibits a discernible red-shift in the Soret band to 450 nm. This notable shift is attributed to the extended $\pi$ conjugation facilitated by the two-dimensional framework of the COFs,[21] leading to altered electronic transitions and spectral properties compared to the precursor molecule, Zn-TAPP.

We analyzed the $CO_2$ adsorption capacity of MPOR-COFs (M = $H_2$, $Zn^{2+}$, $Cu^{2+}$) synthesized with and without pyridine, and the results are presented in Figure 3. $CO_2$ sorption data was collected using a QCM at 20 °C and 50 psi operating pressure; the details are provided in the Supporting


https://doi.org/10.1021/acsaenm.4c00285
ACS Appl. Eng. Mater. 2024, 2, 1743−1747

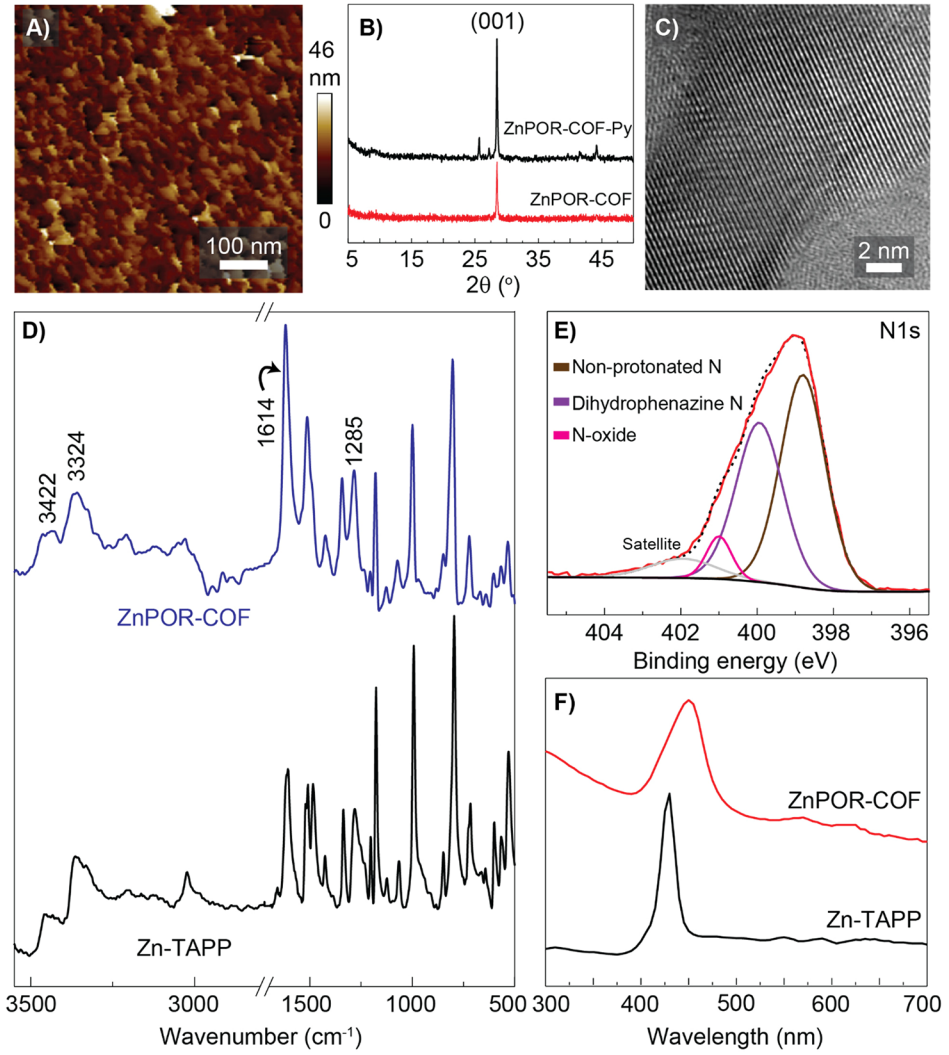


**Figure 2.** Characterization of Zn-TAPP and ZnPOR-COF thin film: A) Atomic force microscope (AFM) height images of ZnPOR-COF-coated QCM crystal. B) Powder X-ray diffraction (PXRD) of ZnPOR-COF and ZnPOR-COF-Py deposited on sapphire. C) High-resolution transmission electron microscope (HRTEM) image of ZnPOR-COF-Py. D) Attenuated total reflection Fourier transform infrared spectroscopy (ATR-FTIR) of Zn-TAPP and ZnPOR-COF. E) X-ray photoelectron spectroscopy (XPS) high-resolution N 1s spectrum of ZnPOR-COF. F) UV−vis spectra of Zn-TAPP and ZnPOR-COF deposited on quartz. The Zn-TAPP deposition rate was 7.0 nm $s^{-1}$.

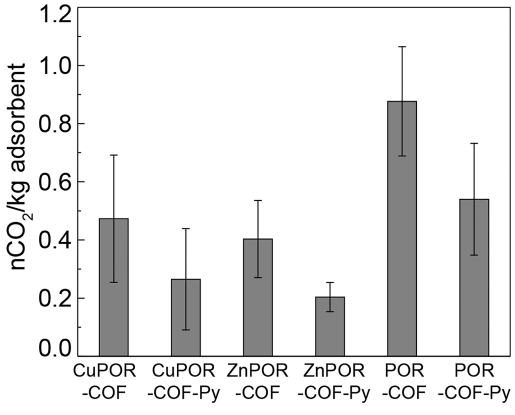


**Figure 3.** Estimation of $CO_2$ sorption using quartz crystal microbalance: The $CO_2$ adsorption capacity of MPOR-COF is evaluated at 20 °C and 50 psi. The error bars represent the average measured values from six samples, and the data is reported with one standard deviation.

Information, Section 3. POR-COF exhibited higher $CO_2$ uptake, averaging 0.88 ± 0.18 mol of $CO_2$/kg compared to POR-COF-Py, which showed 0.54 ± 0.19 mol of $CO_2$/kg of adsorbent. This observation suggests that the increase in the crystallinity of COFs reduces their $CO_2$ adsorption capacity. Conversely, COFs with metal active centers, such as CuPOR-COF and ZnPOR-COF, showed compromised $CO_2$ absorption, which can be attributed to the reduced active sites within their 2D lattice structure. The $CO_2$ uptake for CuPOR-COF and ZnPOR-COF were measured to be 0.47 ± 0.21 and 0.40 ± 0.13 mol of $CO_2$/kg of adsorbent, respectively. The lower values for the $CO_2$ uptakes of CuPOR-COF-Py and ZnPOR-COF-Py, were measured to be 0.26 ± 0.17 and 0.20 ± 0.05 mol of $CO_2$/kg of adsorbent, respectively. As discussed in Figure 1E and Figure S4, an increase in crystallinity was accompanied by an increase in crystallite size. The higher $CO_2$ uptake for the less crystalline sample was observed. This trend mirrors the findings of Ma et al.,[22] who noted that flexible COF-300 exhibited reduced $N_2$ and Ar uptake as the crystallite size increased. Additionally, the reduced crystallinity can be related to the incomplete reaction of the precursor molecule,



https://doi.org/10.1021/acsaenm.4c00285
ACS Appl. Eng. Mater. 2024, 2, 1743−1747

which forms amorphous domains within the films, leaving unreacted primary terminal amine groups for attracting $CO_2$ molecules through acid−base pair formation.[23]

We estimated the enthalpy of adsorption (-Δ*H*) for MPOR-COFs using the Clausius−Clapeyron equation via 24-point adsorption isotherms. The details are presented in the supporting document. The estimated -Δ*H* for POR-COF was 8.79 ± 1.02 kJ/mol of $CO_2$, falling within the enthalpy of adsorption in physisorption, indicating lower energy required for stripping off the $CO_2$ molecule. The -Δ*H* for ZnPOR-COF and CuPOR-COF were 14.66 ± 0.84 kJ/mol and 12.14 ± 1.51 kJ/mol, respectively. We attributed the increased values of -Δ*H* for the metal-containing COFs to the affinity of the metal center in the porphyrin moiety to attract $CO_2$. This observation aligns with the reported adsorption energy of $CO_2$ by metalloporphyrin: −15.87 kJ/mol and −17.95 kJ/mol, for Cu−N−C and Zn−N−C, respectively.[24] Figure S6 compares the range of $CO_2$ uptake measured in this work against the heat of adsorption with existing data for MOFs/COFs and cross-linked polymers. While materials with higher $CO_2$ sorption are typically preferred for carbon capture, it is equally crucial to consider lower adsorption kinetics, as they can enhance adsorbent recyclability and decrease the energy consumption needed for regeneration. To gain deeper insights into the $CO_2$ adsorption mechanism of the MPOR-COF, we opted for the Langmuir[25] and Freundlich isotherm models, and the parameters were deduced through curve-fitting. The outcomes of this analysis are detailed in the Supporting Information, Section 3. From the Freundlich model and using the heterogeneity theory, we noted that the MPOR-COFs heterogeneity ($n^{-1}$) is higher for the materials containing transition metal elements.[26] The estimated equivalent surface heterogeneity (n-1) values were 1.81, 2.20, and 2.40 for POR-COF, CuPOR-COF, and ZnPOR-COF, respectively.

Figure 4 illustrates a trend for the excess molar concentration of 1.75 and 2.75 (mole $CO_2$ per kg of adsorbent) in POR-COF, CuPOR-COF, and ZnPOR-COF, plotted against the natural log of pressure and the inverse of temperature at steady-state conditions using point adsorption isotherms at varying temperatures (e.g., 10 to 40 °C) and pressures (e.g., 50 to 200 psi). The higher isosteric heats of adsorption ($Q_{st}$) values for 2.75 excess moles compared to 1.75 are attributed to $CO_2$ molecules occupying favorable sites first, enhancing the mutual attraction of $CO_2$ molecules on the adsorbent surface with increased adsorbate concentration. This is in line with the previous report by Ariana et al.,[27] showing that the isosteric heat of adsorption increases as a function of mass loading if the excess moles undergo favorable molecular interactions with the framework and the surrounding particles until saturation.

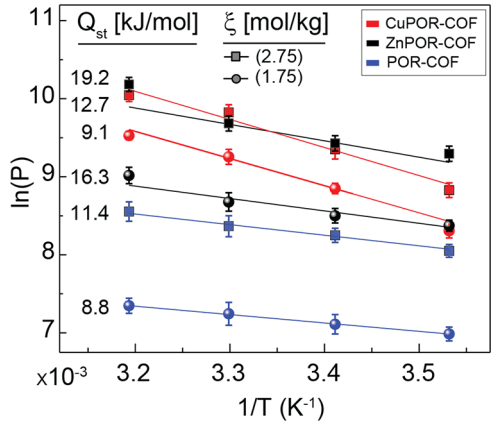


**Figure 4.** A graph displaying the natural logarithm of pressure, ln (P), plotted against the reciprocal of temperature (1/T) for two different excess molar concentrations (ξ) of (○) 1.75 and (□) 2.75 mol $CO_2$/kg adsorbent. The estimated isosteric heat of adsorptions, in KJ per mole and for each concentration, are shown. The error bars represent the average measured values from three samples, and the data is reported with one standard deviation.

In summary, we examined the $CO_2$ sorption capacity of thin films of porphyrin-based covalent organic frameworks (MPOR-COFs) synthesized through vapor-phase oxidative polymerization. Our experimental findings demonstrated that POR-COF outperformed ZnPOR-COF and CuPOR-COF in $CO_2$ uptake, with values of 0.88 ± 0.18, 0.47 ± 0.21, and 0.40 ± 0.13 mol of $CO_2$/kg of adsorbent, respectively. Additionally, we assessed the $CO_2$ adsorption capacity of MPOR-COFs synthesized with and without pyridine, revealing contrasting trends in crystallinity and $CO_2$ uptake. While POR-COF exhibited higher $CO_2$ uptake, averaging 0.88 ± 0.18 mol of $CO_2$/kg of adsorbent, POR-COF-Py showed 0.54 ± 0.19 mol of $CO_2$/kg of adsorbent, suggesting that increased crystallinity marginally reduced $CO_2$ adsorption capacity. Furthermore, our data elucidate the variation in the enthalpy of adsorption as a function of the occupancy of the porphyrin center. These insights underscore the tunability of $CO_2$ interaction with the porphyrin-based networks and offer valuable insights for advancing selective separation media.

## ■ ASSOCIATED CONTENT

### Supporting Information

The Supporting Information is available free of charge at https://pubs.acs.org/doi/10.1021/acsaenm.4c00285.

General experimental procedures and characterizations including TEM, AFM, FT-IR, and $CO_2$ adsorption isotherm (PDF)

## ■ AUTHOR INFORMATION


### Corresponding Authors

**Mona Bavarian** − *Department of Chemical and Biomolecular Engineering, University of Nebraska-Lincoln, Lincoln, Nebraska 68588, United States;* orcid.org/0000-0001-7689-773X; Email: mona.bavarian@unl.edu

**Siamak Nejati** − *Department of Chemical and Biomolecular Engineering, University of Nebraska-Lincoln, Lincoln, Nebraska 68588, United States;* orcid.org/0000-0002-1807-2796; Email: snejati2@unl.edu

### Authors

**Syed Ibrahim Gnani Peer Mohamed** − *Department of Chemical and Biomolecular Engineering, University of Nebraska-Lincoln, Lincoln, Nebraska 68588, United States;* orcid.org/0000-0001-9460-8620

**Sarang Ismail** − *Department of Chemical and Biomolecular Engineering, University of Nebraska-Lincoln, Lincoln, Nebraska 68588, United States;* orcid.org/0009-0004-4662-8044

**Ahmed El-Harairy** − *Department of Chemical and Biomolecular Engineering, University of Nebraska-Lincoln, Lincoln, Nebraska 68588, United States; Environmental,*




https://doi.org/10.1021/acsaenm.4c00285
ACS Appl. Eng. Mater. 2024, 2, 1743−1747

*Energy, and Green Chemistry Laboratory, Faculty of Agriculture, Damietta University, Damietta 34517, Egypt*

Complete contact information is available at: https://pubs.acs.org/10.1021/acsaenm.4c00285

### Author Contributions

[§]S.I.G.P.M. and S.I. contributed equally to this work. Conceptualization: S.N. and M.B. Methodology: S.I.G.P.M., S.N., M.B., and S.I., and A.E.H. Investigation: S.I.G.P.M., S.N., S.I., and M.B. Funding acquisition: S.N. and M.B. Project administration: S.N. and M.B. Supervision: S.N. and M.B. Writing: S.I.G.P.M, S.I. and A.E.H. Writing-reviewing and editing; S.N., M.B., S.I.G.P.M., S.I. Additional editing: during revision A.E.H. added a secondary affiliation to the manuscript. All authors have read and approved the final manuscript

### Notes

The authors declare no competing financial interest.

## ■ ACKNOWLEDGMENTS

This research is supported by the National Science Foundation (NSF) and the Americal Chemical Society-Petroleum Research Fund (ACS-PRF) under the award numbers #2047291 and #66227-DNI4, respectively. The authors acknowledge using the Nebraska Nanoscale Facility: National Nanotechnology Coordinated Infrastructure and the Nebraska Center for Materials and Nanoscience, supported by the National Science Foundation under Award ECCS: 1542182 and the Nebraska Research Initiative.

## ■ REFERENCES

(1) Rudd, J. A. An Industrial Take on Developing and Deploying Carbon Capture at Scale. *Nat. Rev. Chem.* **2024**, *8* (1), 1−2.
(2) Sun, X.; Zhang, Q.; Li, S.; Zhang, Y.; Liu, M.; He, B.; Mei, Y.; Zu, Y. Maximizing the Utilization of Calcium Species in the Supercages of CaNa-FAU Zeolite for Efficient CO2 Capture. *Chem. Eng. J.* **2024**, *481*, No. 148661.
(3) Ramos, P. B.; Mamaní, A.; Erans, M.; Jerez, F.; Ponce, M. F.; Sardella, M. F.; Arencibia, A.; Bavio, M. A.; Sanz-Pérez, E. S.; Sanz, R. CO2 Capture from Porous Carbons Developed from Olive Pruning Agro-Industrial Residue. *Energy Fuels* **2024**, *38* (7), 6102−6115.
(4) Liu, S.; Wang, L.; Zhang, H.; Fang, H.; Yue, X.; Wei, S.; Liu, S.; Wang, Z.; Lu, X. Efficient CO2 Capture and Separation in MOFs: Effect from Isoreticular Double Interpenetration. *ACS Appl. Mater. Interfaces* **2024**, *16* (6), 7152−7160.
(5) Konduru, N.; Lindner, P.; Assaf-Anid, N. M. Curbing the Greenhouse Effect by Carbon Dioxide Adsorption with Zeolite 13X. *AIChE J.* **2007**, *53* (12), 3137−3143.
(6) Li, G.; Xiao, P.; Webley, P.; Zhang, J.; Singh, R.; Marshall, M. Capture of CO 2 from High Humidity Flue Gas by Vacuum Swing Adsorption with Zeolite 13X. *Adsorption* **2008**, *14*, 415−422.
(7) Wang, Y.; Kang, C.; Zhang, Z.; Usadi, A. K.; Calabro, D. C.; Baugh, L. S.; Yuan, Y. D.; Zhao, D. Evaluation of Schiff-Base Covalent Organic Frameworks for CO2 Capture: Structure−Performance Relationships, Stability, and Performance under Wet Conditions. *ACS Sustain. Chem. Eng.* **2022**, *10* (1), 332−341.
(8) Li, H.; Dilipkumar, A.; Abubakar, S.; Zhao, D. Covalent Organic Frameworks for CO 2 Capture: From Laboratory Curiosity to Industry Implementation. *Chem. Soc. Rev.* **2023**, *52* (18), 6294−6329.
(9) Wu, S.; Li, Y.; Wang, T.; Li, H.; Wang, X.; Ma, L.; Zhang, N.; Yue, P.; Li, Y. Design and Synthesis of Dual Functional Porphyrin-Based COFs as Highly Selective Adsorbent and Photocatalyst. *Chem. Eng. J.* **2023**, *470*, No. 144135.
(10) Sonea, A.; Crudo, N. R.; Warren, J. J. Understanding the Interplay of the Brønsted Acidity of Catalyst Ancillary Groups and the Solution Components in Iron-Porphyrin-Mediated Carbon Dioxide Reduction. *J. Am. Chem. Soc.* **2024**, *146* (6), 3721−3731.
(11) Wang, C.; Song, X.; Wang, Y.; Xu, R.; Gao, X.; Shang, C.; Lei, P.; Zeng, Q.; Zhou, Y.; Chen, B.; Li, P. A Solution-Processable Porphyrin-Based Hydrogen-Bonded Organic Framework for Photoelectrochemical Sensing of Carbon Dioxide. *Angew. Chem., Int. Ed.* **2023**, *62* (43), No. e202311482.
(12) Mu, X.; Liu, Y.; Xiao, G.; Xu, C.; Gao, X.; Cao, J. Porphyrin Supramolecule as Surface Carrier Modulator Imparts Hole Transporter with Enhanced Mobility for Perovskite Photovoltaics. *Angew. Chem.* **2023**, *135* (39), No. e202307152.
(13) Suresh, R.; Vijayakumar, S. Adsorption of Greenhouse Gases on the Surface of Covalent Organic Framework of Porphyrin−An Ab Initio Study. *Phys. E Low-Dimens. Syst. Nanostructures* **2021**, *126*, No. 114448.
(14) Mohamed, S. I. G. P.; Namvar, S.; Zhang, T.; Shahbazi, H.; Jiang, Z.; Rappe, A. M.; Salehi-Khojin, A.; Nejati, S. Vapor-Phase Synthesis of Electrocatalytic Covalent Organic Frameworks. *Adv. Mater.* **2024**, *36* (14), No. 2309302.
(15) Baltus, R. E.; Culbertson, B. H.; Dai, S.; Luo, H.; DePaoli, D. W. Low-Pressure Solubility of Carbon Dioxide in Room-Temperature Ionic Liquids Measured with a Quartz Crystal Microbalance. *J. Phys. Chem. B* **2004**, *108* (2), 721−727.
(16) Nguyen, T. S.; Hong, Y.; Dogan, N. A.; Yavuz, C. T. Gold Recovery from E-Waste by Porous Porphyrin−Phenazine Network Polymers. *Chem. Mater.* **2020**, *32* (12), 5343−5349.
(17) Walter, M. G.; Wamser, C. C. Synthesis and Characterization of Electropolymerized Nanostructured Aminophenylporphyrin Films. *J. Phys. Chem. C* **2010**, *114* (17), 7563−7574.
(18) Hu, Y.; Goodeal, N.; Chen, Y.; Ganose, A. M.; Palgrave, R. G.; Bronstein, H.; Blunt, M. O. Probing the Chemical Structure of Monolayer Covalent-Organic Frameworks Grown via Schiff-Base Condensation Reactions. *Chem. Commun.* **2016**, *52* (64), 9941−9944.
(19) Muralidharan, S.; Hayes, R. G. Intense Satellites in the N 1s X-Ray Photoelectron Spectra of Certain Metalloporphyrins. *J. Am. Chem. Soc.* **1980**, *102* (15), 5106−5107.
(20) Niwa, Y.; Kobayashi, H.; Tsuchiya, T. X-ray Photoelectron Spectroscopy of Tetraphenylporphin and Phthalocyanine. *J. Chem. Phys.* **1974**, *60* (3), 799−807.
(21) Parvatkar, P. T.; Kandambeth, S.; Shaikh, A. C.; Nadinov, I.; Yin, J.; Kale, V. S.; Healing, G.; Emwas, A.-H.; Shekhah, O.; Alshareef, H. N.; Mohammed, O. F.; Eddaoudi, M. A Tailored COF for Visible-Light Photosynthesis of 2,3-Dihydrobenzofurans. *J. Am. Chem. Soc.* **2023**, *145* (9), 5074−5082.
(22) Ma, T.; Wei, L.; Liang, L.; Yin, S.; Xu, L.; Niu, J.; Xue, H.; Wang, X.; Sun, J.; Zhang, Y.-B.; Wang, W. Diverse Crystal Size Effects in Covalent Organic Frameworks. *Nat. Commun.* **2020**, *11* (1), 6128.
(23) Huang, N.; Krishna, R.; Jiang, D. Tailor-Made Pore Surface Engineering in Covalent Organic Frameworks: Systematic Functionalization for Performance Screening. *J. Am. Chem. Soc.* **2015**, *137* (22), 7079−7082.
(24) Wang, Y.; Yang, Z.; Zhang, N.; Wang, D.; Wang, R.; Peng, W.; Zhang, J.; Liu, J.; Zhang, J. CO2 Capture and Separation with Metalloporphyrin Nanosheets in an Electric Field: A DFT Study. *Appl. Surf. Sci.* **2023**, *610*, No. 155340.
(25) Yang, A.; Wang, Z.; Zhu, Y. Facile Preparation and Adsorption Performance of Low-Cost MOF@cotton Fibre Composite for Uranium Removal. *Sci. Rep.* **2020**, *10* (1), 19271.
(26) Shikuku, V. O.; Mishra, T. Adsorption Isotherm Modeling for Methylene Blue Removal onto Magnetic Kaolinite Clay: A Comparison of Two-Parameter Isotherms. *Appl. Water Sci.* **2021**, *11* (6), 103.
(27) Torres-Knoop, A.; Poursaeidesfahani, A.; Vlugt, T. J. H.; Dubbeldam, D. Behavior of the Enthalpy of Adsorption in Nanoporous Materials Close to Saturation Conditions. *J. Chem. Theory Comput.* **2017**, *13* (7), 3326−3339.